(1976).
14. A. Blumenthal, P. Bissinger, H. Schmidbaur, *J. Organomet. Chem.* **462**, 107 (1993).
15. T. Imamoto, T. Hikosaka, *J. Org. Chem.* **59**, 6753 (1994).
16. M. Unverzagt *et al.*, *Angew. Chem. Int. Ed. Engl.* **36**, 1469 (1997).
17. H. Braunschweig, M. Colling, *Coord. Chem. Rev.* **223**, 1 (2001).
18. G. J. Irvine *et al.*, *Chem. Rev.* **98**, 2685 (1998).
19. M. Wagner, N. J. R. van Eikema Hommes, H. Nöth, P. v. R. Schleyer, *Inorg. Chem.* **34**, 607 (1995).
20. K. E. Laidig, A. Streitwieser, *J. Comput. Chem.* **17**, 1771 (1996).
21. A. J. Arduengo III, R. L. Harlow, M. Kline, *J. Am. Chem. Soc.* **113**, 361 (1991).
22. H.-W. Wanzlick, *Angew. Chem. Int. Ed. Engl.* **1**, 75 (1962).
23. N. Metzler-Nolte, *New J. Chem.* **22**, 793 (1998).
24. A. Sundermann, M. Reiher, W. W. Schoeller, *Eur. J. Inorg. Chem.* **1998**, 305 (1998).
2005), pp. 117–137.
28. E. S. Schmidt, A. Jockisch, H. Schmidbaur, *J. Am. Chem. Soc.* **121**, 9758 (1999).
29. M. B. Abrams, B. L. Scott, R. T. Baker, *Organometallics* **19**, 4944 (2000).
30. L. Weber *et al.*, *Chem. Ber.* **130**, 705 (1997).
31. I. L. Fedushkin *et al.*, *Eur. J. Inorg. Chem.* **2003**, 3336 (2003).
32. L. Weber *et al.*, *Eur. J. Inorg. Chem.* **1999**, 491 (1999).
33. J. Emsley, *The Elements* (Oxford Univ. Press, New York, ed. 3, 1998), pp. 40, 52.
34. A. J. Arduengo III, R. Krafczyk, R. Schmutzler, *Tetrahedron* **55**, 14523 (1999).
35. A. J. Arduengo *et al.*, *J. Am. Chem. Soc.* **116**, 6361 (1994).
36. N. P. Rath, T. P. Fehlner, *J. Am. Chem. Soc.* **110**, 5345 (1988).
37. The related compounds, Cy_3P-BH_2-CH(OH)Ph, have been reported by the reaction of Cy_3P-BH_2Li with PhCHO in (*15*).
38. Diaminoboryllithium $[(H_2N)_2BLi]$ was calculated to react

41. We thank I. Kawashima and K. Goto for the use of an x-ray diffractometer for **4**, and N. Tokitoh and T. Sasamori for data processing of **3**-DME. Supported by Grant-in-Aid for Scientific Research on Priority Areas 17065005 (Advanced Molecular Transformations of Carbon Resources) and for Young Scientists (B 18750027) from Ministry of Education, Culture, Sports, Science and Technology, Japan, and by a Takeda Pharmaceutical Company Award in Synthetic Organic Chemistry. Structural parameters for compounds **3**-DME, **4**, and **11** are available free of charge from the Cambridge Crystallographic Data Centre under numbers CCDC-604926, 611434, and 604927, respectively.

Supporting Online Material

www.sciencemag.org/cgi/content/full/314/5796/113/DC1
Materials and Methods
Figs. S1 and S2
Table S1

29 June 2006; accepted 25 August 2006
10.1126/science.1131914

Unraveling the Mystery of Indian Monsoon Failure During El Niño

K. Krishna Kumar,[1] Balaji Rajagopalan,[2,3] Martin Hoerling,[4]* Gary Bates,[4] Mark Cane[5]

The 132-year historical rainfall record reveals that severe droughts in India have always been accompanied by El Niño events. Yet El Niño events have not always produced severe droughts. We show that El Niño events with the warmest sea surface temperature (SST) anomalies in the central equatorial Pacific are more effective in focusing drought-producing subsidence over India than events with the warmest SSTs in the eastern equatorial Pacific. The physical basis for such different impacts is established using atmospheric general circulation model experiments forced with idealized tropical Pacific warmings. These findings have important implications for Indian monsoon forecasting.

Climate is the decisive influence on habitation and subsistence of India's burgeoning population. India's wealth is measured by its agricultural output, and now even modest harvest failures result in exaggerated economic and societal consequences. Swings in crop abundances are propelled by the year-to-year successes of the summer (June to September) monsoon rains (*1*). As a result, monsoon predictions are achieving new importance for setting into motion timely and effective preparedness and mitigation activities. The predictions themselves can be as influential as the actual verified monsoon rainfall, as happened for Zimbabwe during 1997 when drought predictions led to curtailment of bank loans for agricultural development (*2*). A similar situation, also during 1997, occurred in India when a much-touted prediction of poor monsoon rains proved false. A more painful scenario unfolded during 2002 and 2004 (*3*, *4*) when normal monsoon rains were predicted but severe drought materialized for which no contingencies were in place.

In many seasonal forecast tools, Indian monsoon rains are predicted to vary in direct proportion to the strength of the El Niño Southern Oscillation (ENSO) phenomenon in the tropical Pacific (*5*–*7*), measured, for example, by the standardized NINO3 index (*8*). Indeed, years with moderate to extreme cold states (NINO3 index < –1), have had abundant monsoon rains without exception. On the other hand, years of moderate to extreme warm states have not been reliably dry. As seen in Fig. 1, the six leading droughts (*8*) since 1871 have occurred in tandem with a standardized NINO3 index exceeding +1, but the presence of El Niños has not guaranteed drought. No simple association describes the relation between the Indian monsoon and NINO3 SSTs when moderate to strong El Niño conditions exist; almost a full range of monsoon rains have accompanied SST warmings. For example, 1997 was the century's strongest El Niño, although no drought occurred, whereas the moderate El Niño of 2002

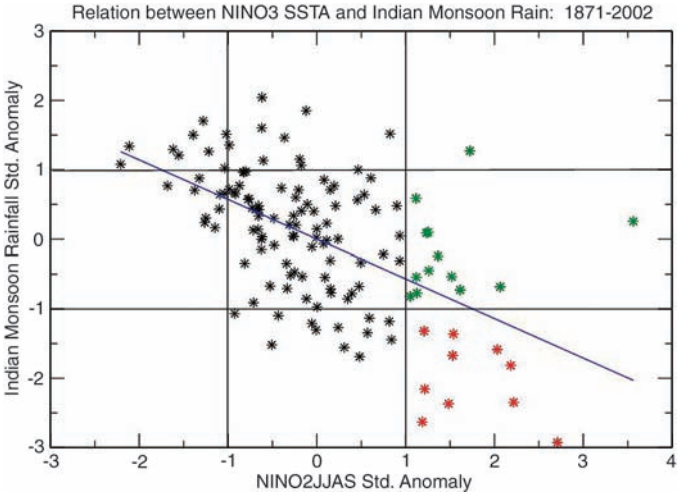

Fig. 1. Plot of standardized, all-India summer [June to September (JJAS)] monsoon rainfall and summer NINO3 anomaly index. Severe drought and drought-free years during El Niño events (standardized NINO3 anomalies > 1) are shown in red and green, respectively.

[1]Indian Institute of Tropical Meteorology, Pune, 411008, India. [2]Department of Civil Environmental and Architectural Engineering, University of Colorado, Boulder, CO 80309, USA. [3]Cooperative Institute for Research in Environmental Sciences, University of Colorado, Boulder, CO 80309, USA. [4]National Oceanic and Atmospheric Administration, Earth System Research Laboratory, Boulder, CO 80305, USA. [5]Lamont-Doherty Earth Observatory, Columbia University, Palisades, NY 10964, USA.

*To whom correspondence should be addressed. E-mail: martin.hoerling@noaa.gov

was accompanied by one of the worst Indian droughts of the past century (*4*). Such ambiguity undermines the utility of monsoon predictions for mitigation of drought's societal impacts.

Two hypotheses have been proposed to explain this ambiguity in the El Niño–Indian monsoon relationship. One is that chaotic variability in rainfall on intraseasonal time scales masks the remote effect of El Niño. Accordingly, the failure (abundance) of monsoon rains during 2002 (1997) would be viewed as the accidental behavior of an inherently noisy monsoon system, and the poor forecasts for these particular cases were the consequence of an only marginally predictable system. The other is that the Indian monsoon is highly sensitive to the details of tropical east Pacific sea surface warming. It is widely believed that El Niño's impact on the Indian monsoon is through the east-west displacement of the ascending and descending branches of the Walker circulation that link Indo-Pacific climates (*9*, *10*). Unusually warm waters during El Niño cause an increased ascent associated with increased rainfall. Mass continuity requires increased descent broadly over southeast Asia, suppressing monsoon rains. The hypothesis we explore is that the strength and position of these branches vary coherently with the details of El Niño warming.

We begin by examining the 23 strong El Niño years for atmosphere and ocean conditions that distinguish the 10 Indian monsoon droughts (red asterisks in Fig. 1) from the 13 drought-free years (green asterisks in Fig. 1). Figure 2A illustrates their contrasting sea surface temperatures (SSTs). The most notable difference in the tropical Pacific SSTs is the greater central Pacific warming during failed Indian monsoon years (Fig. 2A). These analyses suggest that India is more prone to drought when the ocean-warming signature of El Niño extends westward. Figure 2B displays the difference in tropical rainfall for the drought versus drought-free El Niño years. Although rainfall data are based on a smaller sample of cases for which satellite rainfall estimates are available, a physical consistency with the underlying SST anomalies in Fig. 2A is apparent. Increased rainfall occurs over the enhanced warmth of central Pacific Ocean waters, and the satellite estimates confirm dryness over India, the Indian Ocean, and other portions of Southeast Asia, indicating a wide reach to the drought signal. These rainfall anomalies form a dynamical couple that is linked by an Indo-Pacific anomalous Walker circulation, as seen in the velocity potential (*8*) at 200 hPa (Fig. 2B, contours).

The composite anomaly differences highlighted by shading in Fig. 2, A and B, are statistically significant (*8*) and are physically consistent with the expected rainfall-SST relationship. This is further seen by the separability of the probability density functions (PDFs) (*8*) of rainfall for drought versus drought-free years (Fig. 2C). Although this empirical analysis does not establish causal linkages, it does suggest that the two "flavors" of El Niño (*11*) result in significantly different responses in the Indian monsoon. The SST patterns of these two flavors can be described by a linear combination of the two leading, preferred patterns of tropical Pacific SST variability of the past half century (*8*), shown in Fig. 3. The first leading pattern (Fig. 3A) represents the overall strength of the ENSO events, and its associated temporal pattern is highly correlated with fluctuations in the NINO3 index (Fig. 3C). The second pattern (Fig. 3B) has polarity of opposite sign between

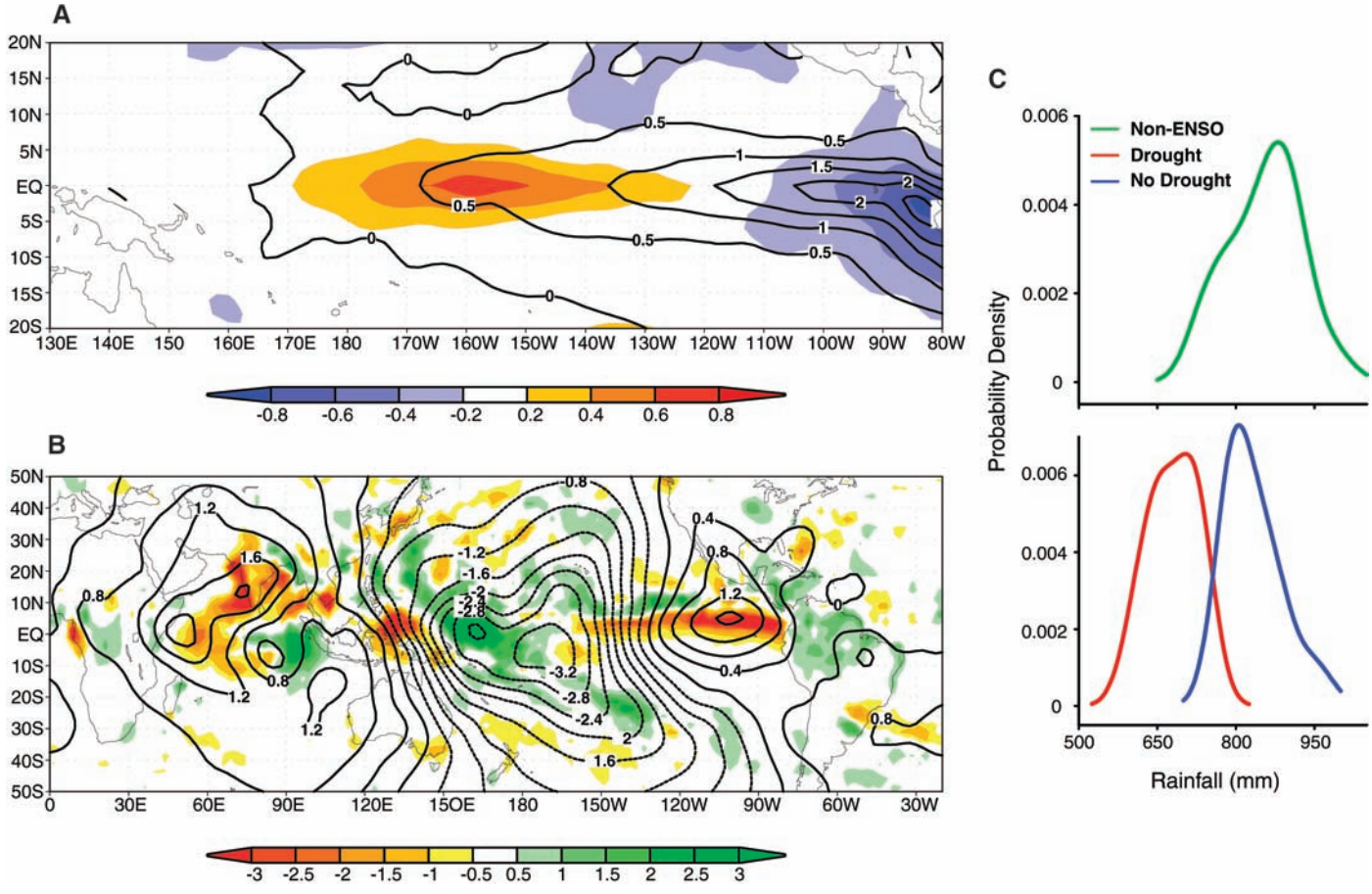

Fig. 2. (**A**) Composite SST difference pattern between severe drought (shaded) and drought-free El Niño years. Composite SST anomaly patterns of drought-free years are shown as contours. (**B**) Composite difference pattern between severe drought and drought-free years of velocity potential (contours) and rainfall (shaded). (**C**) PDF of all-India summer monsoon rainfall from severe-drought (red curve) and drought-free (blue curve) years associated with El Nino occurrence and from the non-ENSO years (green curve). SST and velocity potential composite differences are based on 1950 to 2004, rainfall composites are based on 1979 to 2004, and PDFs are based on 1873 to 2004.

the tropical Central and Eastern Pacific, and its temporal pattern is highly correlated with fluctuations of an index that measures the SST gradient across the Pacific basin (*8*) (Fig. 3D). We note in particular that the second leading pattern closely resembles the SST difference between severe drought and drought-free monsoon years (Fig. 2A, shaded).

General circulation model (GCM) experiments (*8*), forced with SST patterns resulting from linear combinations of the first two leading patterns of tropical Pacific SST variability, are used to test the hypothesis that "westward-shifted" Pacific Ocean warm events drive more intense sinking over the Indian region, initiating severe drought. Using National Center for Atmospheric Research–Community Climate Model Version 3, we performed four ensemble sets of experiments: (i) a 150-year control run of the GCM forced by monthly evolving global climatological mean SST; (ii) a fixed SST pattern resulting from the addition of the first two leading tropical Pacific SST patterns superimposed on the monthly evolving climatological SSTs globally; (iii) same as (ii), but subtracting the second leading tropical Pacific SST pattern from the first; and (iv) an SST pattern corresponding to the first leading pattern (i.e., Fig. 3A) alone. The model experiments for (ii), (iii), and (iv) were performed for a range of imposed SST warmth from 0 to +3 standard deviations (SD), with results available at an interval of 0.2 SD. We analyzed 10 simulations with different initial atmospheric conditions for each of these incremental warmings. Climatological SSTs were prescribed outside the tropical Pacific in these experiments.

Figure 4 illustrates two key aspects of the SST forcing of our atmospheric general circulation model that mimic the empirically derived patterns of Fig. 2. Contours in Fig. 4A are analogous to the amplitude and structure of the composite El Niño SSTs for drought-free years and correspond to the +2 SD experiment described above (iii). Shading in Fig. 4A is analogous to the observed SST structure that discriminates severe drought from drought-free El Niño years and corresponds to the difference between the +2 SD SST forcings of experiments (ii) and (iii). The ensemble mean rainfall and 200 hPa velocity potential difference between experiments (ii) and (iii) are shown in Fig. 4B. Notice a large-scale enhanced drought over the Indian region consistent with enhanced subsidence, and vice versa, in the tropical central Pacific. The similarity of this figure to that noted from the observations (Fig. 2B) is striking. This supports the hypothesis that it is the westward-shifted El Niño events that weaken the Indian monsoon severely.

The behavior of Indian monsoon rainfall under climatological SST conditions (control) and also under the anomalous conditions described by the three different SST patterns of experiments (ii, iii, and iv) is assessed through the construction of PDFs (*8*) that sample all the simulations of Indian rainfall drawn from the separate enactments of the GCM experiments (Fig. 4C).

The PDFs of the experiments using moderate SST warming are not separated, and mean Indian rainfall is only slightly less than the control experiment. For the stronger warming, however, the PDFs of the simulated rainfall are well separated and the median rainfall values are far below those of the control experiment. Under the influence of stronger SST forcing, the PDFs of the experiments that correspond to summing and differencing the two leading tropical Pacific SST patterns fall on the dry and the wet side, respectively, of the median rainfall from the experiment using only the leading SST pattern. This indicates that the leading SST pattern in itself produces droughts in India when of sufficient amplitude, but depending on the sign of the superposed second leading SST pattern, the droughts in India are either strong or weak, with a clear separation in the PDFs.

Identical experiments using two other climate models yield similar results (fig. S1). Also, experiments using the actual SST difference of Fig. 2A (*8*) reproduce the results based on using the idealized SST forcings (fig. S2). For all SST forcings, the PDFs of monsoon rainfall (Fig. 4C) are not sharply peaked but involve a considerable range of possible outcomes. The rainfall spreads are not materially different for the unforced control experiments compared with the strongly forced runs. This illustrates the influence of omnipresent internal atmospheric variability, although such in situ variability alone appears to be insufficient to generate severe monsoon failure.

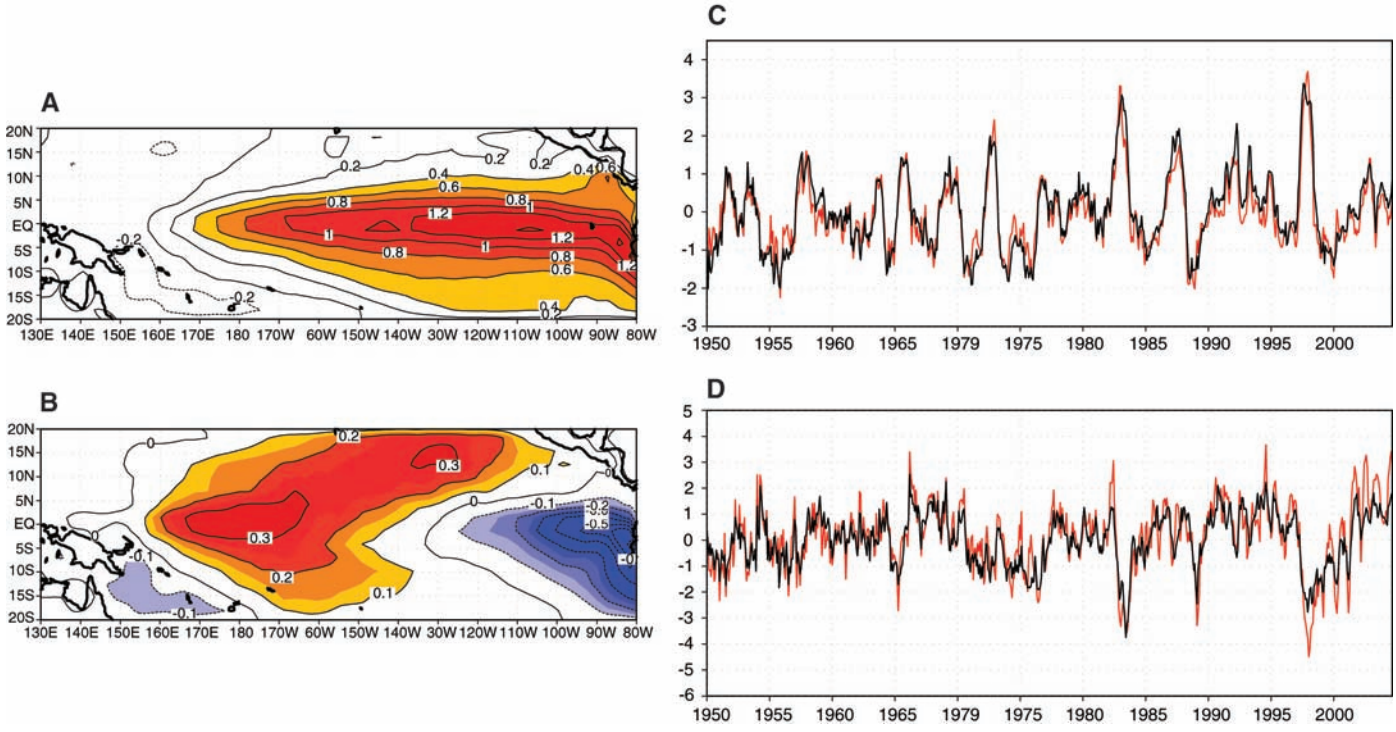

Fig. 3. (**A**) The first leading pattern of the tropical Pacific SST variability. (**B**) Same as (A) but for the second leading pattern. (**C**) The first leading temporal pattern (black line) overlaid with the monthly NINO3 index (red line). (**D**) The second leading temporal pattern (black line) overlaid with the trans-Niño index (TNI) (red line).

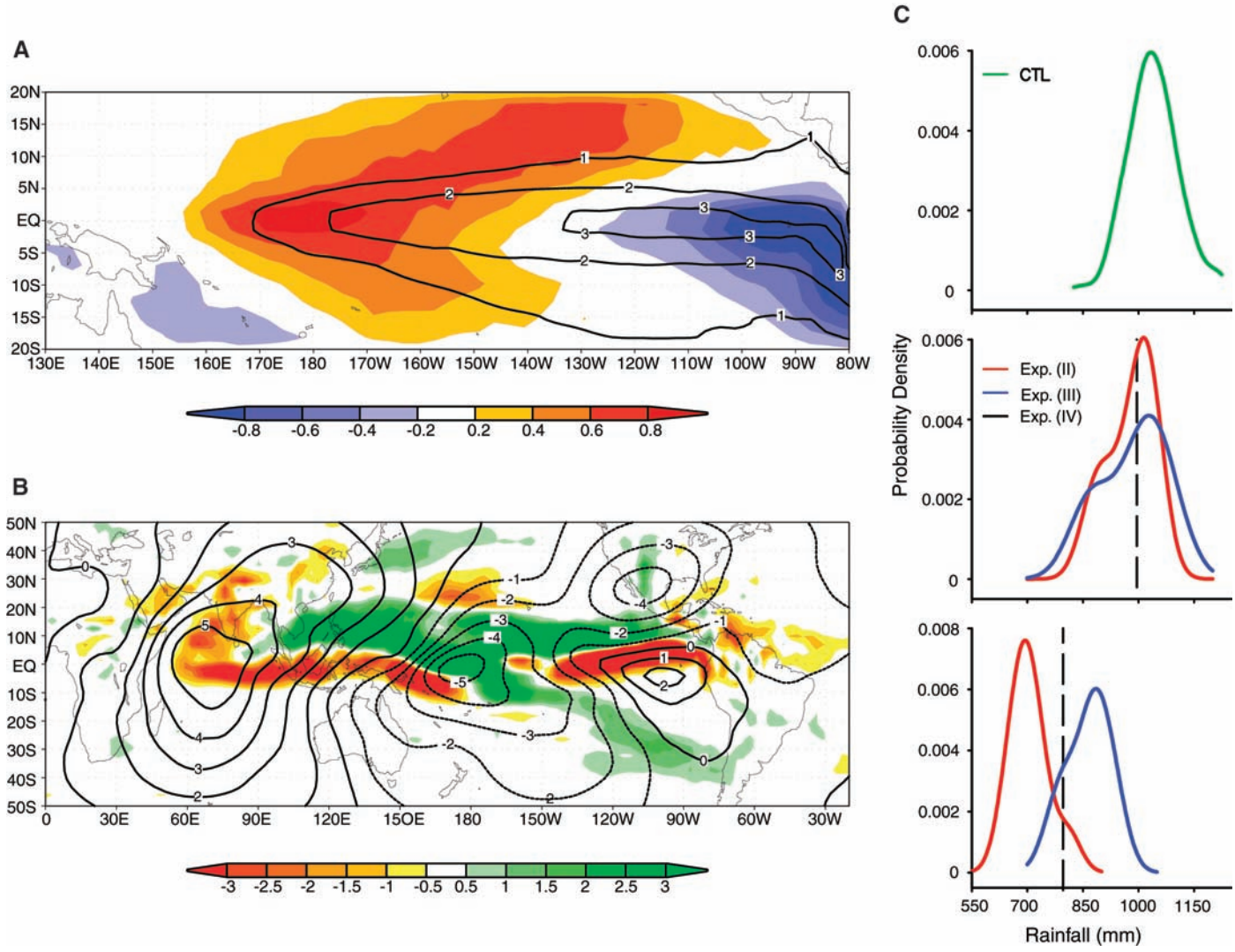

Fig. 4. (**A**) Contours are of the +2 SD experiment (iii) and are analogous to the amplitude and structure of the composite El Niño SSTs for drought-free years in Fig. 2A. Shadings are of the difference between the +2 SD SST forcings of experiments (ii) and (iii) and are analogous to the observed SST structure that discriminates severe drought from drought-free El Niño years. (**B**) The ensemble mean rainfall (shading) and 200 hPa velocity potential (contour) differences between experiments (ii) and (iii). (**C**) The PDF of the Indian monsoon rainfall corresponding to (top) the control, or unforced, experiment (i) green curve; and (middle and bottom) the forced experiments (ii) red curve, (iii) blue curve, and (iv) dashed line with +1 SD (middle) and +2 SD (bottom) imposed SST anomalies. For forced experiment (iv), only the median value (dashed line) is shown. For the forced experiments, each PDF is estimated from 30 ensembles. The model rainfall has been averaged over the Indian monsoon region of 8° to 30°N, 70° to 90°E.

The simulations demonstrate a strong dependence of the Indian monsoon on the tropical Pacific SST anomaly pattern associated with different El Niños. These results do not rule out an independent role for the Indian Ocean, as suggested in other studies (*12*–*14*), or in combination with ENSO (*15*). Regarding the mechanism by which the two flavors of El Niño yield different monsoon impacts, our study has suggested only one candidate, namely, a sensitivity of the tropical Walker circulation. The role of other plausible mechanisms, such as El Niño–monsoon teleconnections from the extratropics (*16*), or the role of reorganized weather disturbances, require further investigation.

The fact that the spatial configuration of tropical Pacific SST anomalies has a significant impact on the Indian monsoon indicates that traditional monsoon forecast methods using predictors that essentially capture the ENSO's strength are likely to be unsuccessful (*17*) in years when the spatial configuration of the SST anomalies is inconsistent with its strength; 1997, 2002, and 2004 are some of the recent years that attest to this. Incorporation of SST configuration information in the statistical models should improve monsoon forecasting skill (fig. S3). There is also the intriguing question of whether either of these flavors of tropical Pacific warmings will become preferred as a consequence of the ocean's response to human-induced changes in Earth's atmosphere's chemical composition. Whereas the consensus of climate change models points to an El Niño–like warming pattern of the tropical Pacific (*18*, *19*), the results of this study indicate that details of that human-induced ocean warming could have material consequences for the monsoon intensity over India.

References and Notes

1. K. Krishna Kumar, K. Rupa Kumar, R. G. Ashrit, N. R. Deshpande, J. W. Hansen, *Int. J. Climatol.* **24**, 1375 (2004).
2. S. G. Philander, *Our Affair with El Niño* (Princeton Univ. Press, Princeton, NJ, 2004).
3. S. Gadgil *et al.*, *Curr. Sci.* **83**, 394 (2002).
4. S. Gadgil, M. Rajeevan, R. Nanjundiah, *Curr. Sci.* **88**, 1389 (2005).
5. S. Hastenrath, *Climate Dynamics of the Tropics* (Kluwer Academic Publishers, Dordrecht, Netherlands, 1991).
6. K. Krishna Kumar, M. K. Soman, K. Rupa Kumar, *Weather* **50**, 449 (1995).
7. J. Shukla, D. A. Paolino, *Mon. Weather Rev.* **111**, 1830 (1983).
8. Materials and methods are available as supporting material on *Science* Online.
9. J. Shukla, in *Monsoons*, J. S. Fein, P. L. Stephens, Eds. (Wiley, New York, 1987).
10. C. F. Ropelewski, M. S. Halpert, *Mon. Weather Rev.* **115**, 1606 (1987).
11. K. Trenberth, *Proc. 18th Ann. Clim. Diagnost. Workshop*, Boulder, CO, **50** (1993).
12. N. H. Saji, B. N. Goswamy, P. N. Vinayachandran, T. Yamagata, *Nature* **401**, 360 (1999).

13. S. Gadgil, P. N. Vinayachandran, P. A. Francis, S. Gadgil, *Geophys. Res. Lett.* **31**, L12213 (2004).
14. K. Krishna Kumar, M. Hoerling, B. Rajagopalan, *Geophys. Res. Lett.* **32**, L08704 (2005).
15. H. Annamalai, P. Liu, *Q. J. R. Meteorol. Soc.* **131**, 805 (2005).
16. B. N. Goswami, P. K. Xavier, *Geophys. Res. Lett.* **32**, L8717, doi: 10.1029/2005GL023216 (2005).
17. K. Krishna Kumar, B. Rajagopalan, M. Cane, *Science* **284**, 2156 (1999).
18. M. A. Cane *et al.*, *Science* **275**, 957 (1997).
19. Intergovernmental Panel on Climate Change, *Climate Change 2001: The Scientific Basis: Summary for Policy Makers and Technical Summary of the Working Group 1 Report* (Cambridge Univ. Press, Cambridge, 2001).
20. We acknowledge funding support from Cooperative Institute for Research in Environmental Sciences and Asia Pacific Network to K.K. and from NOAA's Office of Global Programs to M.H. We also thank T. Xu and J. Eischeid for their contributions.

Supporting Online Material
www.sciencemag.org/cgi/content/full/1131152/DC1
Materials and Methods
Figs. S1 to S3

12 June 2006; accepted 29 August 2006
Published online 7 September 2006;
10.1126/science.1131152
Include this information when citing this paper.

Large Punctuational Contribution of Speciation to Evolutionary Divergence at the Molecular Level

Mark Pagel,* Chris Venditti, Andrew Meade

A long-standing debate in evolutionary biology concerns whether species diverge gradually through time or by punctuational episodes at the time of speciation. We found that approximately 22% of substitutional changes at the DNA level can be attributed to punctuational evolution, and the remainder accumulates from background gradual divergence. Punctuational effects occur at more than twice the rate in plants and fungi than in animals, but the proportion of total divergence attributable to punctuational change does not vary among these groups. Punctuational changes cause departures from a clock-like tempo of evolution, suggesting that they should be accounted for in deriving dates from phylogenies. Punctuational episodes of evolution may play a larger role in promoting evolutionary divergence than has previously been appreciated.

The theory of punctuated equilibrium as a description of evolution suggests that evolutionary divergence among species is characterized by long periods of stability or stasis followed by short punctuational bursts of evolution associated with speciation. Despite years of work on punctuational change, the theory remains contentious (*1*–*9*), with little or no consensus as to the contribution of punctuational changes to evolutionary divergence. The importance of the theory lies in the challenge it poses for classical accounts of how species diverge.

Punctuational evolution has traditionally been studied in the fossil record. However, phylogenetic trees derived from gene-sequence data contain the signatures of past punctuational and gradual evolution and can be used to study their relative contributions to evolutionary divergence (*10*) (Fig. 1). The nodes of a phylogenetic tree record the number of net-speciation events (speciation-extinction) between the root of the tree and the extant species (Fig. 1, A and B). In phylogenies derived from gene-sequence data, the lengths of the branches of the tree record the expected evolutionary divergence between pairs of speciation events, measured in units of nucleotide substitutions. We denote the sum of the branch lengths between the root of the tree and a species as the path length and write this path length as $x = n\beta + g$, where n is the number of nodes along a path, β is the punctuational contribution of speciation to evolution at each node, and g is the gradual contribution to the path, this being the sum of the individual gradual effects in each branch along the path. Both parameters are measured in units of expected nucleotide substitutions per site in the gene-sequence alignment. Under a gradual model of evolution, there is no punctuational effect, $\beta = 0$, and there should be no relationship between x and n (Fig. 1, B and C). If, however, speciation events are associated with bursts of evolution, then $\beta > 0$, and path lengths from the root to the tips of the tree will be correlated with the number of speciation events that occur along that path (Fig. 1, A and C).

We analyzed 122 gene-sequence alignments selected for including a well-characterized and narrow taxonomic range of species (*11*). This acts to control for background differences among species, such as generation times or adaptive radiation of some lineages, that might affect rates of evolution independently of a punctuational effect. For each data set, we derived a Bayesian sample of the posterior distribution of phylogenetic trees (*11*, *12*). We then estimated β from the relationship between x and n in each tree in the posterior sample to account for phylogenetic uncertainty, using a statistical method (*10*, *13*–*15*) that controls for the shared inheritance of branch lengths implied by the phylogeny (Fig. 1)

Using conservative statistical criteria (*11*), we found a significant relationship between nodes and path lengths (i.e., $\beta > 0$) in 57 [46.7 ± 4.5% (±SE)] of the 122 trees. We removed 22 of these data sets with $\beta > 0$ because they suffered from an artifact of phylogeny reconstruction known as the node-density effect, which can produce an apparent relationship between x and n (*10*, *11*, *16*–*18*). This left 35.0 ± 4.8% of the remaining 100 trees with significant effects of punctuational evolution (Fig. 2), rising to 55.8 ± 7.0% for trees above the median size of $n = 28$ taxa. The overall frequency of 35% is similar to that found in the subset of trees in which 50% of the known taxa have been

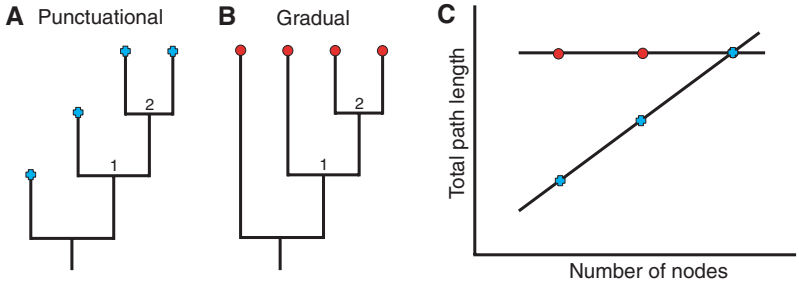

Fig. 1. Signatures of punctuational and gradual evolution on phylogenetic trees. (**A**) Punctuational evolution presumes a burst of evolution associated with each node of the tree. Path lengths, measured as the sum of branches along a path from the root to the tips of the tree, are proportional to the number of nodes along that path (C). Branches are assumed to be in units of nucleotide substitutions. (**B**) Gradual evolution presumes that change is independent of speciation events. Path lengths do not correlate with the number of nodes along a path (C). (**C**) Punctuational evolution predicts a positive relationship between path length and the number of nodes, whereas gradual evolution does not.

School of Biological Sciences, University of Reading, Whiteknights, Reading RG6 6AJ, UK.

*To whom correspondence should be addressed. E-mail: m.pagel@rdg.ac.uk